

RSC Advances



This is an *Accepted Manuscript*, which has been through the Royal Society of Chemistry peer review process and has been accepted for publication.

Accepted Manuscripts are published online shortly after acceptance, before technical editing, formatting and proof reading. Using this free service, authors can make their results available to the community, in citable form, before we publish the edited article. This *Accepted Manuscript* will be replaced by the edited, formatted and paginated article as soon as this is available.

You can find more information about *Accepted Manuscripts* in the [Information for Authors](#).

Please note that technical editing may introduce minor changes to the text and/or graphics, which may alter content. The journal's standard [Terms & Conditions](#) and the [Ethical guidelines](#) still apply. In no event shall the Royal Society of Chemistry be held responsible for any errors or omissions in this *Accepted Manuscript* or any consequences arising from the use of any information it contains.



CLIC1 antibody conjugated nano-scale contrast agent as a sensitive and targeted molecular imaging probe for gallbladder cancer diagnosis

Received 00th January 20xx,
Accepted 00th January 20xx

DOI: 10.1039/x0xx00000x

www.rsc.org/

Wei Lu,^{#a,d} Ning Wang,^{#b} YanYan Chu,^b Linzhu Zhou,^c Maolan Li,^{a,d} Tao Huang,^e Hao Weng,^{a,d} Yijian Zhang,^{a,d} Lin Jiang,^{a,d} Yunping Hu,^{a,d} Qinggang Tan,^{*b} Yingbin Liu,^{*a,d}

Limited by current clinical diagnosis techniques, gallbladder cancer remains a highly lethal disease and is associated with an extremely poor prognosis and treatment outcome. In an effort to overcome these severe obstacles, targeted nano-scale contrast agents have been developed and used in the past to increase the sensitivity and specificity of cancer detection. The development of targeted nano-scale contrast agents would offer an even more promising approach for gallbladder cancer diagnosis and subsequent treatment. In this study, a targeted nanoscale contrast agent was developed by conjugation of a CLIC1 antibody to carboxylated multi-walled carbon nanotubes (MWCNTs). Using a gallbladder cancer tumor xenograft model, it could be shown that intravenous injection of this tumor-targeted contrast agent to tumor-bearing mice exhibited a rapid photoacoustic signal with high intensity, leading to contrast enhancement of the entire tumor region. Mice injected with an untargeted contrast agent did not exhibit obvious tumor enhancement. We were able to show that CLIC1 antibody-conjugated to nano-scale contrast agents prove to be highly beneficial for this fast and sensitive imaging technique for gallbladder tumors. Taken in concert, the results obtained indicate that the development of targeted nanoscale imaging probes offers a promising approach for the early detection and subsequent treatment of gallbladder cancer.

1. Introduction

Gallbladder cancer (GBC) represents the most frequently occurring malignancy of the biliary system. The tumorous lesions prove to be highly aggressive, often associated with an early onset of metastasis due to the genetic characteristics displayed by this cancer type.¹ Early identification and precise diagnosis, together with radical surgical resection are currently the only efficient treatment modalities available for GBC.^{2,3} However, due to limited ways to identify lymph node metastasis states or near organ invasions of disease stage conditions, GBC remains highly lethal and is often associated with an extremely poor prognosis.⁴ Even though great improvements of abdominal imaging modalities have

been made in recent years, including high resolution computer tomography or magnetic resonance imaging systems,^{5,6} the precise diagnosis of the metastasis state of GBC still remains a critical goal. Therefore, an urgent need exists for the development of innovative approaches providing high sensitivity and accuracy in the early diagnosis of GBC. The use of contrast enhancing imaging agents may increase the sensitivity of a given imaging technique. In particular, nano-scale contrast enhancing agents have been shown to potentially offer high resolution and enhanced sensitivity of cancer diagnosis due to enhanced permeation and retention (EPR) effects resulting in the desired accumulation of the contrast agent in solid tumors.⁷⁻¹⁶ Moreover, nano-scale contrast enhancing agents may be covalently linked to biorecognition molecules such as peptides, antibodies and nucleic acids to target tumor tissues through ligand-receptor interactions.¹⁷⁻²⁸ Such efforts are especially important for the enhancement specificity and sensitivity of cancer detection and may further assist in accurate tumor staging for the appropriate selection of subsequent treatment modalities.

CLIC1 (Chloride Intracellular channel, CLIC) belongs to the family of chloride intracellular channel that have been demonstrated recently to feature profound physiological functions.²⁹⁻³¹ In particular, it was found that CLIC1 can exist in different forms and in various positions, which has been shown to be closely related to malignant tumor types.^{32,33} Furthermore, it has been reported that CLIC1

^a Department of General Surgery, Xinhua Hospital, Affiliated to Shanghai JiaoTong University, School of Medicine, 1665 Kongjiang Road, Shanghai 200092, China. Email: liuybphd@126.com

^b College of Materials Science and Engineering, Key Laboratory for Advanced Civil Engineering Materials (Ministry of Education), Tongji University, Caoan Road 4800, Shanghai 201804, P. R. China. Email: qgtan@tongji.edu.cn

^c School of Chemistry and Chemical Engineering, Shanghai Jiao Tong University, 800 Dongchuan Road, 200240 Shanghai, P.R. China.

^d Institute of Biliary Tract Diseases Research, Shanghai JiaoTong University School of Medicine, 1665 Kongjiang Road, Shanghai 200092, China.

^e KoGuan Law School of Shanghai Jiao Tong University, 800 Dongchuan Road, 200240 Shanghai, P.R. China.

These authors contributed equally to this work

plays an important role in malignant tumor invasion and metastasis.³⁴ Our previous study demonstrated that the expression of CLIC1 is significantly up-regulated in the highly metastatic gallbladder cancer cell and the overexpression is also associated with poor prognosis in gallbladder cancer.^{32,35} Therefore, this channel represents an interesting target and effective biomarker for predicting the prognosis of gallbladder cancer.

Nano-scale contrast enhancing agents combined with the CLIC1 antibody might be of great value in the diagnosis of gallbladder cancer via accurate prediction of the prognosis and subsequent selection of a suitable therapeutic regimen. Due to their intrinsic optical properties, carbon nanotubes (CNTs) have been shown to be potentially useful as contrast agents to be used in a variety of biomedical imaging techniques.³⁶⁻⁴⁰ In particular, the strong absorbance features in the near-infrared (NIR) region render CNTs potentially useful as photoacoustic imaging contrast agents.^{39, 40} In this present study, we selected carbon nanotubes conjugated with CLIC1 antibodies as photoacoustic imaging contrast agents in an effort to explore the potential for the development of targeted nano-probes that could be used to visually diagnose gallbladder cancer *in vivo*. To evaluate the potential of nano-scale contrast agents combined with the CLIC1 antibody for the diagnosis of gallbladder cancer, an *in vivo* gallbladder cancer xenograft tumor model in nude mice was selected. We could demonstrate that the intravenous administration of the tumor-targeted contrast agent to tumor-bearing mice results in a rapid and strong enhancement of the photoacoustic signal in the tumor. No significant signal enhancement could be observed in mice injected with an untargeted contrast agent. The results obtained indicate that a sufficient amount of the nano-scale contrast agent covalently linked with CLIC1 antibodies may rapidly accumulate in the tumor, potentially useful for sensitive gallbladder cancer imaging. Taken in concert, the findings presented here provide precious insights into the overall understanding of using CLIC1 antibody-conjugated contrast agents to increase enhancement specificity and sensitivity in the detection of GBC. The results obtained may assist in accurate tumor staging for the selection of efficient treatment strategies.

2. Materials and methods

2.1 Materials

Carboxylated multi-walled carbon nanotubes (carboxylic acid MWCNTs, diameter = 20-30 nm, length = 0.5-2 μm , -COOH content = 1.23 wt%) were purchased from Chengdu organic chemicals company (China); Polyethyleneimine (PEI, Mn=10000), 1-ethyl-3-[3-(dimethylamino)propyl]carbodiimide hydrochloride (EDC, Mw = 191.7 g mol⁻¹ \geq 99%), N-hydroxysulfosuccinimide sodium salt (Sulfo-NHS, Mw = 217.1 g mol⁻¹, \geq 99%) and anti-CLIC1 antibody (produced in mouse) were purchased from Sigma-Aldrich (St. Louis, USA). Poly (ethyleneglycol) distearoyl phosphatidylethanolamine (PEG-DSPE, Mn=5000) was purchased from Shenzhen Xingjiafeng Technology Co. Ltd. (China). Phosphate-buffered saline (PBS) was purchased from Shanghai Yuanye biological

technology company (China). Deionized water was used as the solvent in all aqueous solutions. Fetal bovine serum, DMEM and William's medium E cell culture medium were purchased from Gibco. The human GBC cell lines were purchased from the Cell Bank of the Chinese Academy of Sciences (Shanghai, China).

2.2 Preparation of PEI-MWCNTs

30 mg of carboxylated multi-walled carbon nanotubes were dispersed in 50 mL deionized water by sonication for 30 minutes and 1 g of branched PEI was dispersed in 100 ml deionized water under stirring. Next, the dispersed MWCNTs solution was added to the PEI aqueous solution (10 mg mL⁻¹) dropwise under stirring. The mixed solution was then transferred into a round-bottom flask and reacted at 60 °C using an oil bath for 24 hours. After reaction, the suspension was cooled to room temperature and was washed with deionized water three times and was centrifuged at 10,000 rpm to remove any residual PEI. The resulting PEI-MWCNTs aqueous solution was stored at low temperature (4°C).

2.3 Preparation of PEG-DSPE/PEI-MWCNTs

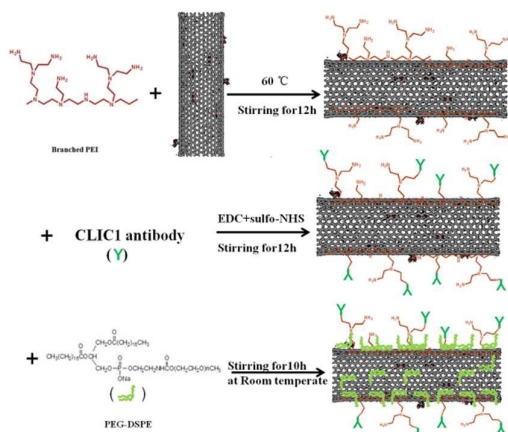
20 mg of PEG-DSPE powder was dissolved in 20 mL deionized water. Upon stirring, the dispersed PEI-MWCNTs were added dropwise to the resulting aqueous solution of PEG-DSPE (1 mg mL⁻¹). After reaction for 20 hours, the suspension was washed with deionized water and centrifuged at 8,000 rpm to remove any residual PEG-DSPE. The resulting solution of PEG-DSPE/PEI-MWCNTs was stored at low temperature (4°C).

2.4 Preparation of PEG-DSPE/CLIC1 antibody- PEI-MWCNTs

Briefly, EDC (8 mg, 40 μmol) and sulfo-NHS (5 mg, 40 μmol) were dissolved in 3 ml deionized water at 0 °C before addition of the antibody solution (100 μL , 1 mg mL⁻¹). After 30 minutes, the aqueous solution of PEI-MWCNTs was added and stirred at room temperature for 12 hours. EDC in the presence of sulfo-NHS converts the carboxylic acid groups on the CLIC1 antibody to amine-reactive sulfo-NHS esters. These esters may then further react with any available amine groups on the surface of PEI-MWCNTs, thus conjugating the antibody to the PEI functionalized MWCNTs via formation of stable covalent amide bonds. After the reaction was completed, the resulting samples were added dropwise to the aqueous solution of PEG-DSPE (1 mg mL⁻¹) and were stirred for 2 hours. The reaction mixtures were then centrifuged at 8000 rpm for 10 minutes and the resulting PEG-DSPE/CLIC1 antibody-PEI-MWCNTs were resuspended in PBS and were stored at low temperature (4°C) until further use.

2.5 Characterization of contrast agents

The dispersions of carboxylated MWCNTs, PEI-MWCNTs and PEG-DSPE/PEI-MWCNTs were first characterized using a digital camera, and were further studied via transmission electron microscopy (TEM, FEI, Japan). The samples for TEM analysis were prepared by placing 0.5 ml of the suspensions onto a plain copper grid and air-drying the grid at room temperature. TEM analysis was then performed on a JEM-1200EX TEM, operating at 200 kV in bright field mode. The chemical structures of the samples were analyzed via X-ray



Scheme 1. Schematic representation of the preparation process of PEG-DSPE/CLIC1 antibody-PEI-MWCNTs.

photoelectron spectroscopy (XPS) and fourier transform infrared spectroscopy (FTIR). The chemical composition of the samples was provided by an ESCALAB MARK spectrometer by using Mg Ka exciting radiation. High-resolution spectra of C1s, N1s, and O1s were obtained. FTIR spectra were recorded on a Bruker EQUINOX55 spectrometer and samples were pressed into potassium bromide (KBr) pellets.

2.6 Tumor xenograft model

The media for cell lines were supplemented with 10% fetal bovine serum (FBS) and 1% penicillin-streptomycin (10,000 U/ml penicillin and 10 mg/ml streptomycin). The GBC cells were incubated at 37°C in a humidified atmosphere with 5% CO₂. Male immunodeficient BALB/c nude mice (6 weeks old) were purchased from the Shanghai Laboratory Animal Centre of the Chinese Academy of Sciences and raised in the experimental animal centre of Xinhua Hospital and all experiments were performed in accordance with the guidelines of the Institutional Animal Care and Use Committee of Shanghai Jiao Tong University.

A subcutaneous xenograft metastasis tumor model was established as following: well status GBC cells were cultured in vitro. The cells were collected and digested using trypsin (0.25% (w/v) Trypsin- 0.53 mM EDTA solution) when grown to 75-85% area of the culture medium. In this study, 5×10⁶ cells were subcutaneously inoculated in the left outer of 6 week old male nude mice. The tumor volume was determined using calipers every 3 days and the total volume was calculated according to the following formula: tumor volume (mm³) = (L × W²)/2 (L and W represent the length and width of the tumors, respectively). When the tumor reached 5-20 mm in diameter, the mass could be detected via photoacoustic imaging.

2.7 Photoacoustic imaging

Ten tumor-bearing nude mice were randomly and equally classified into 2 groups, and then contrast agents were injected into the tail vein of the tumor-bearing mice at a dose of 0.2 mL. Photoacoustic imaging was performed on a Nexus 128 system (ENDRA Inc., Ann Arbor, MI, USA) at pre-injection, at 5 minutes, at 1 hour, at 2 hours, and at 24 hours post-injection. Light with wavelengths of 800 nm,

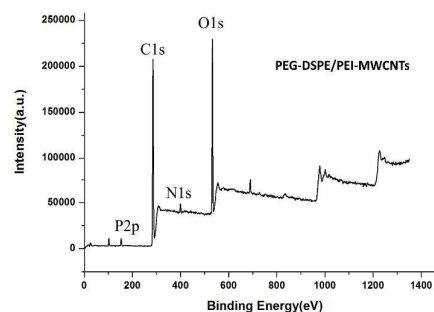
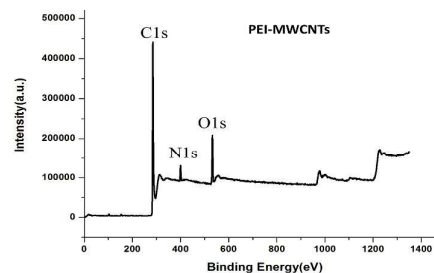
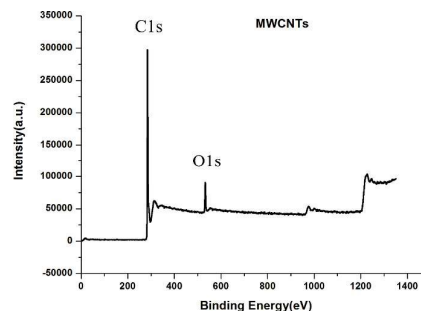


Figure 1. XPS survey scan spectra for different modified MWCNTs.

830 nm and 890 nm were generated using a wavelength-tunable laser to excite the photoacoustic signals.

3. Results and discussion

The entire conjugation procedure of the CLIC1 antibody onto the surface of MWCNTs can be found summarized in Scheme 1. Polyethyleneimine (PEI) was covalently conjugated onto carboxylated MWCNTs via amide formation between the amine groups and the carboxylic acid groups. Upon covalent amide formation, the MWCNTs were equipped with more primary amines, suitable for further covalent conjugation of the antibody. The CLIC1 antibody was then bioconjugated to the PEI functionalized MWCNTs using 1-ethyl-3-[3-(dimethylamino) propyl]carbodiimide hydrochloride (EDC) as a crosslinking agent in the presence of N-hydroxysulfosuccinimide sodium salt (sulfo-NHS). To further increase the circulation half-life and simultaneously reduce the nonspecific accumulation rate in healthy tissue, polyethylene glycol (PEG) groups were

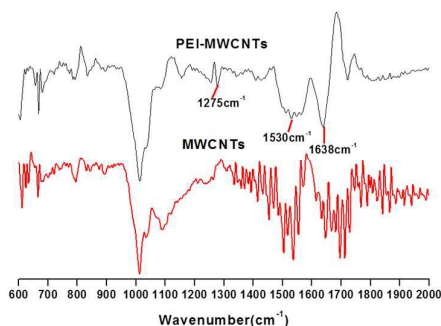


Figure 2. FT-IR spectra for MWCNTs and PEI-MWCNTs.

introduced to the surface of the antibody-conjugated MWCNTs via non-covalent modification with phospholipid poly (ethylene glycol) (PL-PEG).

XPS is a surface-sensitive quantitative chemical analysis technique that can be used to analyze the surface chemistry of a material in its as-received state or upon treatment. Here, the structural parameters of the modified MWCNTs were first characterized by X-ray photoemission spectroscopy (XPS). Figure 1 shows the XPS spectra for the carboxylic acid MWCNTs, PEI-MWCNTs and PEG-DSPE/PEI-MWCNTs. As can be seen by inspection of Figure 1a, the carboxylic acid MWCNTs exhibit two main peaks, corresponding to C1s and O1s, while the appearance of an N peak in the XPS survey spectrum for PEI-MWCNTs compared to that of carboxylic acid MWCNTs provides evidence for the adsorption of PEI chains onto the surface of MWCNTs. As expected, a new peak corresponding to P2p appears in the XPS survey spectrum for PEG-DSPE/PEI-MWCNTs and the ratio of O1s/C1s also improved compared to that of PEI-MWCNTs or carboxylic acid MWCNTs. The latter finding demonstrates that both PEI and PEG-DSPE are successfully introduced onto the surface of MWCNTs, as outlined in Scheme 1. The chemical structures were further characterized by FT-IR. As shown in Figure 2, the typical absorption peaks of the amide bond (amide I band: $\nu_{C=O}=1638\text{ cm}^{-1}$, amide II band: $\nu_{N-H}=1530\text{ cm}^{-1}$, amide III band: $\nu_{C-N}=1275\text{ cm}^{-1}$) were observed in the spectrum of the PEI-MWCNTs which demonstrated the PEI molecules was successfully introduced onto the surface of MWCNTs via the amide formation between the amine groups and the carboxylic acid groups.

The dispersed properties of the as-obtained conjugates were characterized using a digital camera. Optical images of the dispersion of carboxylic acid MWCNTs, PEI-MWCNTs and PEG-DSPE/MWCNTs in phosphate buffer solution are shown in Figure 3. Pristine carboxylic acid MWCNTs could be dispersed in aqueous solution and prove to be stable for approximately 3 days (data not shown here). However, in PBS the carboxylic acid MWCNTs precipitate immediately. The formed dispersion of PEI-modified MWCNTs and PEG-DSPE/PEI-MWCNTs in PBS was shown to be stable without the occurrence of any obvious precipitation, even after several weeks of storage. Precipitation of the carboxylic acid MWCNTs is most likely

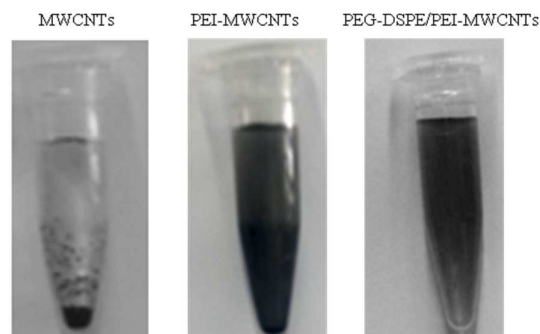


Figure 3. Images of different modified MWCNTs dispersed in PBS solution.

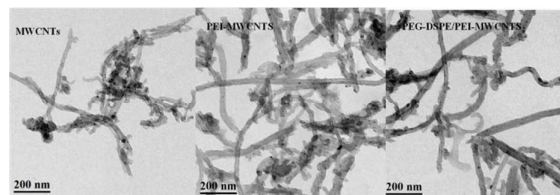


Figure 4. TEM images of different modified MWCNTs.

caused by ionic properties from dissociated salts in PBS, leading to a reduction of the electrostatic repulsion between the carboxylic MWCNTs. In PBS, the ionic strength also reduces the electrostatic repulsion of PEI molecules; however, the PEI molecule chain features primary, secondary and tertiary amino groups. These may be protonated depending on the pH and the individual pKa value of the amines, potentially leading to a stronger electrostatic repulsion of the PEI molecules and a stable dispersion of MWCNTs in PBS. Further adsorption of the non-ionic surfactant (DSPE) onto the surface of PEI-MWCNTs could not only improve the dispersion characteristics of the MWCNTs, but also leads to a decreased effect of the ionic strength in the dispersion. The effect of surface modification on the dispersion of MWCNTs was further studied using TEM. As shown in Figure 4, MWCNTs that were directly dispersed in deionized water formed large bundles and were prone to aggregation. After PEI and DSPE functionalization, the MWCNTs were found to be mostly separated into individual nanotubes. Similar results were found for MWCNTs in solution. The results obtained from TEM analysis indicate that the modified MWCNTs exhibit a well-defined nano-structure, representing another crucial feature for the development of nano-scale contrast enhancing agents.

The specificity and efficacy of the CLIC1 antibody-conjugated nano-scale contrast agent were evaluated in living mice. Mice bearing tumor xenografts were administered 200 μL of either PEG-DSPE/PEI-MWCNTs (untargeted control) or PEG-DSPE/CLIC1 antibody-PEI-MWCNTs (targeted) at a concentration of 0.5 mg ml^{-1} via tail vein injection. Imaging was performed for more than 120 minutes post-injection of the contrast agent to determine in vivo dynamics.

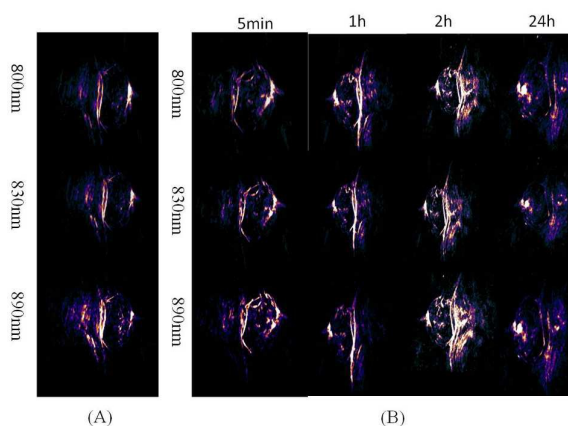


Figure 5. Photoacoustic images of a gallbladder metastatic tumor before (A) and after (B) injection of PEG-DSPE/PEI-MWCNTs.

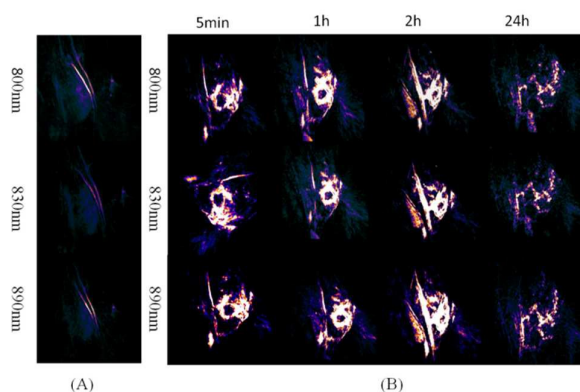


Figure 6. Photoacoustic images of a gallbladder metastatic tumor before (A) and after (B) injection of PEG-DSPE/CLIC1 antibody-PEI-MWCNTs.

As indicated in Figure 5A, the photoacoustic signals in the tumors (wavelengths 800, 830, and 890 nm) using the control were found to be weak and only vague structural tumor silhouettes could be detected in combination with several bright long strips (i.e. main blood vessels) scattered across the whole region. The photoacoustic signal in the tumor before injection is primarily caused by the high blood content in the tumor region. Exemplary images of the tumor 5 minutes post-injection of PEG-DSPE/PEI-MWCNTs show no obvious changes compared to the images of the control (cf. Figure 5B). The photoacoustic signal in the tumors appears to be somewhat improved 1 hour post-injection, as shown in Figure 5. However, compared to the control, the photoacoustic signal in the tumor proves to be significantly more intense in mice injected with PEG-DSPE/PEI-MWCNTs 2 hours post-injection. The overall silhouette of the tumor becomes more distinct and can clearly be identified. At later stages (i.e. 24 hours post-injection), however, this situation was found to be reversed, with the photoacoustic signal in the tumor found to be

almost similar to that of the control and the early stage (i.e. 5 minutes post-injection).

Interestingly, 5 minutes post-injection of the PEG-DSPE/CLIC1 antibody-PEI-MWCNTs, the photoacoustic signals in the tumor (wavelengths 800, 830 and 890 nm) were found to be significantly intensified and the outline of tumor could also be clearly identified, as shown in Figure 6. Furthermore, it should be noted in this context that in contrast to mice injected with PEG-DSPE/PEI-MWCNTs, the photoacoustic signal in the central area of the tumor proves to be very intense, exhibiting a continuously bright area. As a consequence, no obvious long strips stemming from blood vessels could be detected. The photoacoustic signal in the tumor was further improved at the 1 hour time point post-injection and the outline of tumor also becomes clearer, as indicated in Figure 6. After 2 hours post-injection, a more intense photoacoustic signal was detected, with almost the entire silhouette of the tumor region clearly enhanced. The photoacoustic signal in the tumor 24 hours post-injection of PEG-DSPE/CLIC1 antibody-PEI-MWCNTs also decreased similarly to that of the control sample.

Commonly accepted in the literature is the fact that nanomaterials can penetrate the tumor vasculature through a permeable endothelium. The general lack of lymphatic drainage in tumors often results in the accumulation of extravascular nanomaterials within the tumor tissues. This so-called enhanced permeation and retention (EPR) effect may enable nanomaterials to passively target tumor tissues. Upon injection of PEG-DSPE/PEI-MWCNTs as passively targeted probes, the construct is believed to accumulate in the tumor via this EPR effect. The time-dependent increase in signal amplitude indicates that the PEG-DSPE/PEI-MWCNTs have gradually travelled into the blood stream and nearby tissues. This result indicates that the accumulation of PEG-DSPE/PEI-MWCNTs follow a progressive EPR-mediated effect. However, it should be noted in this context that no signs of early and rapid tumor localization could be detected and the enhanced photoacoustic signal proves to be mainly limited to the corresponding blood vessels and nearby tissues. Instead, intravenous injection of PEG-DSPE/CLIC1 antibody-PEI-MWCNTs in tumor-bearing mice immediately led to significant photoacoustic signal enhancements. The signal also breaks through the overall shape of the blood vessels to form a continuously large bright area. Therefore, the boundaries of the entire tumor region could be also clearly identified.

It is generally appreciated that solid tumors comprise of two interdependent compartments: the parenchyma (neoplastic cells) and the stroma where the neoplastic cells are found to be dispersed. The stroma includes connective tissues, blood vessels, as well as inflammatory cells. Blood vessels represent only one component of the tumor stroma and are usually only a minor component of the overall stromal mass. The interactions of nanomaterials with the intracellular and/or extracellular targets within the tumor environment play a key role in the accumulation of extravascular nanomaterials within tumor tissues. Without these interactions, nanomaterials extravasated from the blood vessels could be easily cleared out from the interstitial space in the tumor in a

relatively short time frame and therefore mainly exist in blood vessels and nearby tissues. For PEG-DSPE/PEI-MWCNTs, there is no specific interaction between the contrast agent and the tumor tissue. Therefore, the enhanced photoacoustic signal mainly reflects the blood vessel of stroma. However, in the case of the PEG-DSPE/CLIC1 antibody-PEI-MWCNTs, the CLIC1 antibody may actively target the CLIC1 receptor on the cell membranes of the tumor. As a consequence, it is likely that the binding and internalization of the PEG-DSPE/CLIC1 antibody-PEI-MWCNTs in CLIC1 expressing tumor cells facilitates the distribution and accumulation of the PEG-DSPE/CLIC1 antibody-PEI-MWCNTs not only in the stroma, but also in the parenchyma of the tumor. Presumably, a sufficient amount of the targeted PEG-DSPE/CLIC1 antibody-PEI-MWCNTs can rapidly accumulate in the tumor, allowing for sensitive tumor imaging.

Enhanced imaging signals disappeared in tumors upon injection of PEG-DSPE/PEI-MWCNTs or PEG-DSPE/CLIC1 antibody-PEI-MWCNTs 24 hours post-injection. This finding is most likely due to the fact that gallbladder tumors prove to be highly invasive and readily disseminate into surrounding tissues. Thus, the interstitial pressure of the tumor may not be high enough to generate a strong retention effect which ultimately results in the contrast agents being cleared out of the interstitial space of the tumor in a relatively long time frame. The time-dependent and slow increase in signal amplitude upon injection of PEG-DSPE/PEI-MWCNTs provides further support for this hypothesis.

Taken together, the above results clearly indicate that conjugating CLIC1 antibodies to nano-scale contrast agents is crucial for the accumulation of a sufficient amount of the targeted contrast agent in the tumor tissue and therefore potentially offers a sensitive gallbladder cancer imaging and efficient diagnosis technique.

4. Conclusions

In summary, CLIC1 targeted nano-scale contrast agents were developed by conjugating CLIC1 antibodies to PEI functionalized MWCNTs. We have successfully demonstrated that the synthesized CLIC1 antibody-conjugated nano-scale contrast agent provides a more intense photoacoustic signal in tumors immediately upon intravenous injection of PEG-DSPE/CLIC1 antibody-PEI-MWCNTs in tumor-bearing mice. The result obtained indicates that active targeting of the CLIC1 receptor present on tumor cells represents a crucial factor for the sufficient accumulation of the targeted nano-scale contrast agent in the GBC tumor for sensitive tumor imaging. These findings demonstrate that CLIC1 antibody-conjugated nano-scale contrast agents may be used in the future as powerful targeted molecular imaging probes for gallbladder cancer diagnosis. Further experimental studies to substantiate this latter notion are currently underway in our laboratory.

Acknowledgements

The authors acknowledge the financial supports from the National High Technology Research and Development Program of China 863 (2012AA022606), the national science foundation of china (No. 91440203, 81172026, 81272402, 81301816, and 81172029), China Postdoctoral Science Foundation (No.2014M561487) and Interdisciplinary Program of Shanghai Jiao Tong University.

Notes and references

- 1 M. Rakic, L. Patrlj, M. Kopljar, R. Kliecek, M. Kolovrat, B. Loncar, Z. Busic, *Hepatobiliary surgery and nutrition*, 2014, **3**, 221-226.
- 2 A. Andren-Sandberg, Y. Deng, *Current opinion in gastroenterology*, 2014, **30**, 326-331.
- 3 J. A. Wernberg, D. D. Lucarelli, *The Surgical clinics of North America*, 2014, **94**, 343-360.
- 4 P. K. Garg, D. Pandey, J. Sharma, *Expert review of gastroenterology & hepatology*, 2015, **9**, 155-166.
- 5 J. Y. Jang, S. W. Kim, S. E. Lee, D. W. Hwang, E. J. Kim, J. Y. Lee, S. J. Kim, J. K. Ryu, Y. T. Kim, *Annals of surgery*, 2009, **250**, 943-949.
- 6 C. H. Tan, K. S. Lim, *Diagnostic and interventional radiology*, 2013, **19**, 312-319.
- 7 E. C. Cho, C. Glaus, J. Chen, M. J. Welch, Y. Xia, *Trends. Mol. Med.*, 2010, **16**, 561-573.
- 8 K. Ding, J. F. Zeng, L. H. Jing, R. R. Qiao, C. Y. Liu, M. X. Jiao, Z. Li, M. Y. Gao, *Nanoscale*, 2015, **7**, 11075-11081.
- 9 U. I. Tromsdorf, N. C. Bigall, M. G. Kaul, O. T. Bruns, M. S. Nikolic, B. Mollwitz, R. A. Sperling, R. Reimer, H. Hohenberg, W. J. Parak, S. Förster, U. Beisiegel, G. Adam, H. Weller, *Nano. Lett.*, 2007, **7**, 2422-2427.
- 10 Y. F. Kong, J. Chen, F. Gao, R. Brydson, B. Johnson, G. Heath, Y. Zhang, Li, Wu, D. J. Zhou, *Nanoscale*, 2013, **5**, 1009-1017.
- 11 J. H. Park, G. Maltzahn, L. Zhang, A. M. Derfus, D. Simberg, T.J. Harris, E. Ruoslahti, S. N. Bhatia, M. J. Sailor, *Small*, 2009, **5**, 694-700.
- 12 H. Liu, H. Wang, Y. H. Xu, M. W. Shen, J. L. Zhao, G. X. Zhang, X. Y. Shi, *Nanoscale*, 2014, **6**, 4521-4526.
- 13 X. Gao, Y. Cui, R. M. Levenson, L. W. Chung, S. Nie, *Nat. Biotechnol.*, 2004, **22**, 969-976.
- 14 G. Maltzahn, J. H. Park, K. Y. Lin, N. Singh, C. Schwöppe, R. Mes-ters, W. E. Berdel, E. Ruoslahti, M. J. Sailor, S. N. Bhatia, *Nat. Mater.*, 2011, **10**, 545-552.
- 15 E. A. Sykes, J. Chen, G. Zheng, W.C.W. Chan, *ACS Nano*, 2014, **8**, 5696-5706.
- 16 X. Wu, X. X. He, K. M. Wang, C. Xie, B. Zhou, Z. H. Qing, *Nanoscale*, 2010, **2**, 2244-2249.
- 17 J. R. McCarthy, J. Bhaumik, M. R. Karver, S. Sibel Erdem, R. Weissleder, *Mol Oncol.*, 2010, **4**, 511-528.
- 18 H. Hu, A. T. Dai, J. Sun, X. Y. Li, F. H. Gao, L. Z. Wu, Y. Fang, H. Yang, L. An, H. X. Wu, S. P. Yang, *Nanoscale*, 2013, **5**, 10447-10454.
- 19 R. M. Lu, Y. L. Chang, M. S. Chen, H. C. Wu, *Biomaterials*, 2011, **32**, 3265-3274.
- 20 H. Y. Chen, S. L. Li, B. W. Li, X. Y. Ren, S. N. Li, D. M. Mahounga, S. S. Cui, Y. Q. Gu, S. Achilefu, *Nanoscale*, 2012, **4**, 6050-6064.
- 21 J. D. Byrne, T. Betancourt, L. Brannon-Peppas, *Adv. Drug Deliv. Rev.*, 2008, **60**, 1615-1626.

- 22 D. Pan, S. D. Caruthers, G. Hu, A. Senpan, M. J. Scott, P. J. Gaffney, S. A. Wickline, G. M. Lanza, *J. Am. Chem. Soc.*, 2008, **130**, 9186-9187.
- 23 Y. Luo, J. Yang, Y. Yan, J. C. Li, M. W. Shen, G. X. Zhang, S. Mignani, X. Y. Shi, *Nanoscale*, 2015, **7**, 14538-14546.
- 24 C. G. Hadjipanayis, R. Machaidze, M. Kaluzova, L. Y. Wang, A. J. Schuette, H. W. Chen, X. Y. Wu, H. Mao, *Cancer Res.*, 2010, **70**, 6303-6312.
- 25 M. Satpathy, L. Y. Wang, R. Zielinski, W. P. Qian, M. Lipowska, J. Capla, G. Y. Lee, H. Xu, A. Wang, H. Mao, L. Yang, *Small*, 2014, **10**, 544-555.
- 26 M. P. Melancon, M. Zhou, R. Zhang, C. Y. Xiong, P. Allen, X. X. Wen, Q. Huang, M. Wallace, J. N. Myers, R. J. Stafford, D. Liang, A. D. Ellington, C. Li, *ACS Nano*, 2014, **8**, 4530-4538.
- 27 M. Corricelli, N. Depalo, E. D. Carlo, E. Fanizza, V. Laquintana, N. Denora, A. Agostiano, M. Striccolib, M. L. Curri, *Nanoscale*, 2014, **6**, 7924-7933.
- 28 F. Chen, H. Hong, Y. Zhang, H. F. Valdovinos, S. X. Shi, G. S. Kwon, C. P. Theuer, T. E. Barnhart, W. B. Cai, *ACS Nano*, 2013, **7**, 9027-9039.
- 29 B. Ulmasov, J. Bruno, P. G. Woost, J. C. Edwards, *BMC cell biology*, 2007, **8**, 8.
- 30 M. Setti, N. Savalli, D. Osti, C. Richichi, M. Angelini, P. Brescia, L. Fornasari, M. S. Carro, M. Mazzanti, G. Pelicci, *Journal of the National Cancer Institute*, 2013, **105**, 1644-1655.
- 31 M. Gritti, R. Wurth, M. Angelini, F. Barbieri, M. Peretti, E. Pizzi, A. Pattarozzi, E. Carra, R. Sirito, A. Daga, R. M. Curmi, M. Mazzanti, T. Florio, *Oncotarget*, 2014, **5**, 11252-11268.
- 32 Q. Ding, M. Li, X. Wu, L. Zhang, W. Wu, Q. Ding, H. Weng, X. Wang, Y. B. Liu, *Tumour Biol.*, 2015, **36**, 193-198.
- 33 Y. Ye, M. Yin, B. Huang, Y. Wang, X. Li, G. Lou, *Tumour Biol.*, 2015, **36**, 4175-4179.
- 34 L. A. Gurski, L. M. Knowles, P. H. Basse, J. K. Maranchie, S. C. Watkins, J. Pilch, *Molecular cancer research*, 2015, **13**, 273-280.
- 35 J. W. Wang, S. Y. Peng, J. T. Li, Y. Wang, Z. P. Zhang, Y. Cheng, D. Q. Cheng, W. H. Weng, X. S. Wu, X. Z. Fei, Z. W. Quan, J. Y. Li, S. G. Li, Y. B. Liu, *Cancer Letters*, 2009, **281**, 71-81.
- 36 M. R. McDevitt, D. Chattopadhyay, B. J. Kappel, J. S. Jaggi, S. R. Schiffman, C. Antczak, J. T. Njardarson, R. Brentjens, D. A. Scheinberg, *J. Nucl. Med.*, 2007, **48**, 1180-1189.
- 37 Z. Liu, W. B. Cai, L. N. He, N. Nakayama, K. Chen, X. M. Sun, X. Y. Chen, H. J. Dai, *Nat. Nanotechnol.*, 2007, **2**, 47-52.
- 38 P. Cherukuri, C. J. Gannon, T. K. Leeuw, H. K. Schmidt, R. E. Smllery, S. A. Curley, R. B. Weisman, *Proc. Natl. Acad. Sci.*, 2003, **103**, 18882-18886.
- 39 A. D. L. Zerda, C. Zavaleta, S. Keren, S. Vaithilingam, S. Bodapati, Z. Liu, J. Levi, B. R. Smith, T. J. Ma, O. Oralkan, Z. Cheng, X. Y. Chen, H. J. Dai, B. T. Khuri-Yakub, S. S. Gambhir, *Nat. Nanotechnol.*, 2008, **3**, 557-562.
- 40 A. Zerda, Z. Liu, S. Bodapati, R. Teed, S. Vaithilingam, B. T. Khuri-Yakub, X. Y. Chen, H. J. Dai, S. S. Gambhir, *Nano. Lett.*, 2010, **10**, 2168-2172.

CLIC1 antibody-conjugated nano-scale contrast agents exhibit a fast and sensitive detection of gallbladder tumors and may be used in the future as powerful targeted molecular imaging probes for gallbladder cancer diagnosis.

